# Satellite-based estimation of total suspended solids and chlorophyll-a concentrations for the Gold Coast Broadwater, Australia

Marine Pollution Bulletin 201 (2024) 116217

Contents lists available at ScienceDirect

Marine Pollution Bulletin

journal homepage: www.elsevier.com/locate/marpolbul

# Satellite-based estimation of total suspended solids and chlorophyll-a concentrations for the Gold Coast Broadwater, Australia

Edoardo Bertone [a,b,c,*], Andrea Ajmar [e], Fabio Giulio Tonolo [d], Ryan J.K. Dunn [b,f], Nicholas J. C. Doriean [b,f], William W. Bennett [b,f,g], Jemma Purandare [b,f,g,h]

[a] School of Engineering and Built Environment, Griffith University, Southport 4215, Queensland, Australia
[b] Cities Research Institute, Griffith University, Southport 4215, Queensland, Australia
[c] Australian Rivers Institute, Griffith University, Nathan 4111, Queensland, Australia
[d] Department of Architecture and Design, Politecnico di Torino, Viale Mattioli, 39, 10125 Torino, Italy
[e] Interuniversity Department of Regional and Urban Studies and Planning (DIST), Politecnico di Torino, Viale Mattioli, 39, 10125 Torino, Italy
[f] Coastal and Marine Research Centre, Griffith University, Southport 4215, Queensland, Australia
[g] School of Environment and Science, Griffith University, Southport 4215, Queensland, Australia
[h] City of Gold Coast, 833 Southport Nerang Road, Nerang 4211, Queensland, Australia

ARTICLE INFO

*Keywords:*
Chlorophyll-*a*
Empirical modelling
Remote sensing
Total suspended solids
Water quality

ABSTRACT

Satellite retrieval of total suspended solids (TSS) and chlorophyll-*a* (*chl-a*) was performed for the Gold Coast Broadwater, a micro-tidal estuarine lagoon draining a highly developed urban catchment area with complex and competing land uses. Due to the different water quality properties of the rivers and creeks draining into the Broadwater, sampling sites were grouped in clusters, with cluster-specific empirical/semi-empirical prediction models developed and validated with a leave-one-out cross validation approach for robustness. For unsampled locations, a weighted-average approach, based on their proximity to sampled sites, was developed. Confidence intervals were also generated, with a bootstrapping approach and visualised through maps. Models yielded varying accuracies ($R^2$ = 0.40–0.75). Results show that, for the most significant poor water quality event in the dataset, caused by summer rainfall events, elevated TSS concentrations originated in the northern rivers, slowly spreading southward. Conversely, high *chl-a* concentrations were first recorded in the southernmost regions of the Broadwater.

## 1. Introduction

Remote sensing of water quality through satellite imagery offers unique opportunities for inexpensive, spatially explicit estimation of optically active constituents (OACs) for entire water bodies. Estimation can be completed at relatively high spatial (e.g. 10 or 20 m for most spectral bands of Copernicus Sentinel-2) and temporal (e.g. multiple times each week when combining different satellite data such as from the Sentinel-2 and Landsat missions, assuming there is little to no cloud cover) resolutions (Sagan et al., 2020). Applications of satellite sensing for estimating water quality parameters such as chlorophyll-*a* (*chl-a*) or turbidity have increased in the last decade, as reviewed by Topp et al. (2020).

Micro-tidal estuarine lagoons, such as the Gold Coast Broadwater (hereafter referred to as the Broadwater), are complex systems, hydrodynamically affected both by catchment outflows and marine tides. The Broadwater, which is 25 km in length, receives outflows from four main rivers and several additional creeks, draining diverse catchments, from densely urbanised to grazing/crop lands and dense subtropical rainforest. The Broadwater covers a large area (~32.5 km$^2$) and has considerable spatial variability of water quality parameters (WQP) (Dunn et al., 2007a; Dunn et al., 2012; Dunn et al., 2007b), given the variety of water and potential contaminant inputs and tidal influence. Given the ecological, economic, and cultural importance of the Broadwater, routine water quality monitoring is conducted for numerous purposes, including monitoring ecological health, ensuring human health safety, and as part of regulatory commitments (Dunn et al., 2022). Water quality monitoring programs currently in place are limited by resource constraints and are conducted to comply with legislative requirements and to guide management practices and priorities. Thus,

* Corresponding author at: School of Engineering and Built Environment, Griffith University, Southport 4215, Queensland, Australia.
*E-mail address:* e.bertone@griffith.edu.au (E. Bertone).

https://doi.org/10.1016/j.marpolbul.2024.116217
Received 14 December 2023; Received in revised form 1 March 2024; Accepted 1 March 2024
Available online 22 March 2024

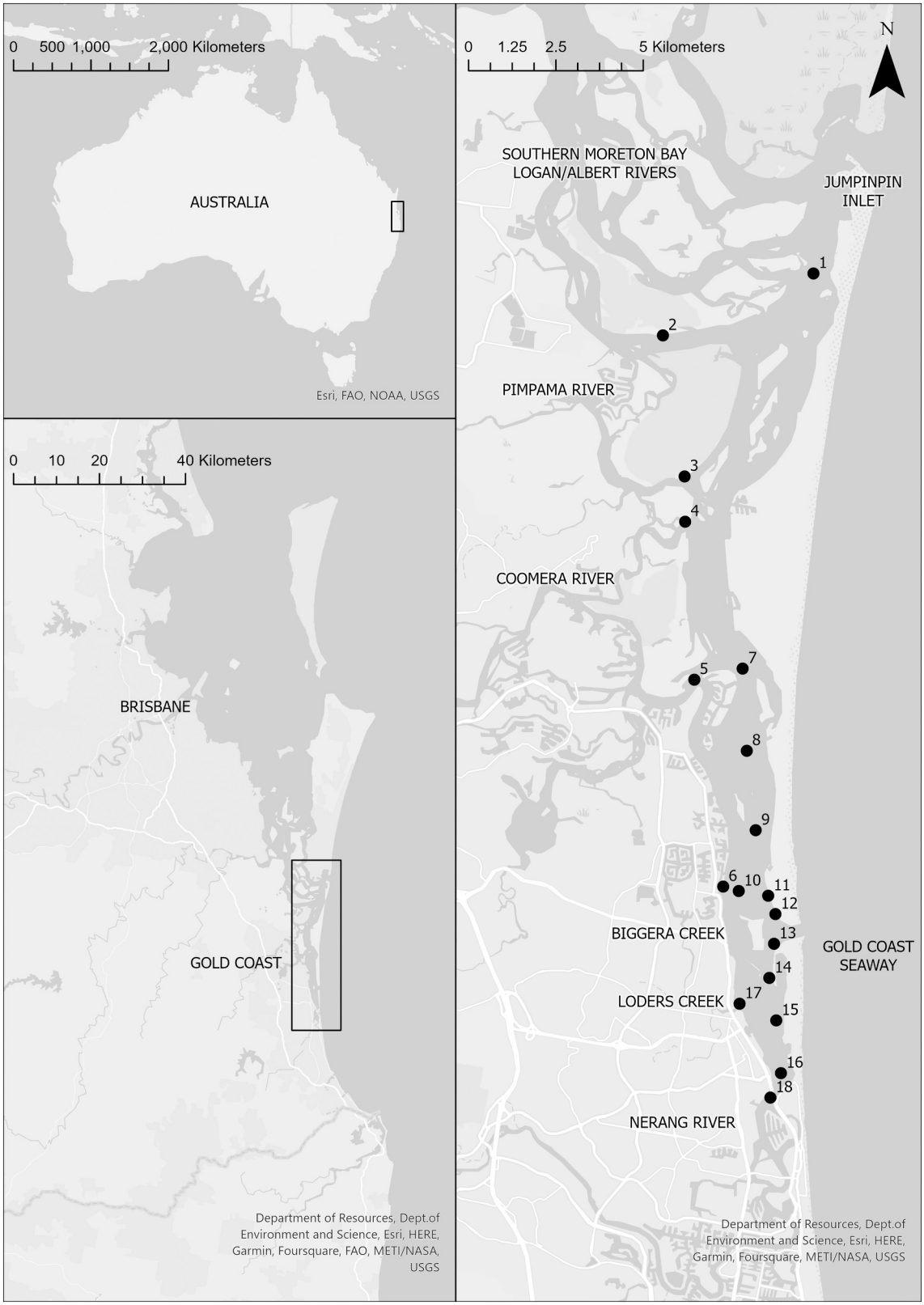


**Fig. 1.** Map of the Broadwater with sampling sites. Adapted from Dunn et al. (2022). In-situ monitoring locations (1–18) are identified with black circles.

the application of a satellite-based, rapid and inexpensive means to estimate water quality for this entire water body would be advantageous. Furthermore, if this could be achieved, it would provide useful data/information regarding satellite-based sensing applications to estuaries/deltas, of which there is a paucity in the scientific literature, as shown in Figs. 1 and 3 in Topp et al. (2020).

A common issue with remote sensing retrieval of water quality parameters such as chlorophyll-a (*chl-a*) and turbidity or total suspended solids (TSS) is the inability of developing a single, universal retrieval model; as such, the majority of developed models are empirical or semi-

empirical (Topp et al., 2020). For instance, for *chl-a*, empirical algorithms use spectral band combinations to estimate concentrations, with potentially high accuracy in local regions or specific inland waters only. However, optical properties are often affected by the presence of other OACs, (e.g., suspended sediments and coloured dissolved organic matter (CDOM)). Likewise, the optical properties of OACs vary independently from *chl-a* in productive inland waters (Dall'Olmo et al., 2005; Kutser et al., 2005). As such, empirical algorithms are typically effective only for specific water body datasets, due to different environmental backgrounds related to the specific biochemical and hydrological characteristics (Li et al., 2021). For instance, in their study, Li et al. (2021) presented a comprehensive modelling methodology for *chl-a* estimation in numerous Chinese lakes. However, their initial step involved employing a *k*-means approach to categorise these lakes into distinct clusters based on their water quality attributes. Subsequently, separate predictive models were developed for each cluster. The performance of their models was dependent on the lake cluster and was influenced by the presence of other non-covarying OACs; in particular, the presence of large amounts of TSS affected the model performance more significantly. Additionally, in the same study, previously published empirical *chl-a* algorithms were tested, with the resulting model accuracy dependent on the features of the different lakes' clusters (Li et al., 2021). Relevant research was also conducted by Cherukuru et al. (2020), who studied TSS retrieval in a coastal site receiving outflows from multiple rivers, and monitoring 26 different sampling sites. They indicated that model performance varied by site due to, among other influences, the spatial variability of backscattering properties of suspended particulate matter, due to varying particle size(s) at different locations, likely related to different origin and in turn composition. In line with these findings, in their work Hansen and Williams (2018) suggested fully data-driven approaches compared to more traditional physics-based *chl-a* modelling, so to exploit information contained in all spectral bands and in turn to help account for lake-specific optical characteristics. Furthermore, Seegers et al. (2021), while successfully developing a generalised algorithm for *chl-a* estimation from Medium Resolution Imaging Spectrometer (MERIS) data for inland lakes in the United States, found the performance varied based on lake characteristics and their trophic state.

As acknowledged in Sagan et al. (2020), different modelling methods have difficulties with transferability and site-specificity. For instance, spectral indices are prone to errors due to interference from other water quality constituents, and they rely on constant (unchanging) water conditions. As such, they are usually recommended for a qualitative assessment of spatial variations of the predicted constituent across the water body, rather than for a direct, quantitative estimation. Similarly, empirical models, despite predicting better in their study, inevitably rely on the data used for calibration/validation. As such, they are representative of the site-specific data and historical variations. The non-generalisability of empirical models is also acknowledged by Topp et al. (2020).

For individual inland water bodies, historical in-situ data from all available sampling sites have typically been used to develop a whole-lake *chl-a* retrieval model. The accuracy of this approach varied greatly from study to study, depending on factors such as lake features; higher accuracies are usually achieved only on eutrophic/hyper-eutrophic lakes (e.g. Duan et al. (2010)). An example related to this work is provided by Bohn et al. (2018) for a shallow Argentinian lake, where good correlation for three sampling sites was achieved for both Secchi Depth and *chl-a* prediction; the latter however fluctuated within a range of approx. 50–850 μg/L. In Markogianni et al. (2018), a model for *chl-a* was developed by combining the results for all sampling sites ($n = 22$), for three sampling dates, for a specific Greek lake. Accuracy for *chl-a* prediction was estimated as $R^2 = 0.33$, highlighting potential challenges in building a generalised satellite-based *chl-a* prediction model, even for a single inland water body.

In addition to site-specificity issues, the quantification and, importantly, visual representation of the model uncertainty is usually lacking; or complex to interpret. Most studies tend to "disconnect" the model development/accuracy estimation from the visual estimation/representation of predictions (Bertone and Peters Hughes, 2023), by refraining from attempting to represent uncertainty during model application/deployment. Recently, Bertone and Peters Hughes (2023) proposed a "one-map" methodological approach, relying on a Bayesian Network prediction modelling framework, to display the probability of exceeding critical operational *chl-a* and turbidity thresholds for a drinking water reservoir. Limited similar alternatives exists, such as visualised in Roncoroni et al. (2022), though without using a Bayesian approach. An alternative method includes the provision of two separate maps, showing respectively (i) the prediction value and (ii) related uncertainty (Werther et al., 2022), which is however less user-friendly to intepret. Other more traditional approaches include calculating confidence intervals; methods to do so include bootstrapping approaches, as applied (also) for this goal by Seegers et al. (2021). All such methods help to quantify uncertainty and thus easily identify varying model accuracy and improvement opportunities (e.g., ranges/sites requiring further data collection).

In this work, we attempt to deal with these shortcomings (i.e. non-generalisability of empirical models and uncertainty representation in model outputs) for a type of water body where satellite-based remote sensing techniques are not commonly utilised (i.e., estuarine lagoons). We suggest a simple spatial distance-based, weighted average approach to incorporate site-specificity while allowing for prediction extrapolation to unmonitored sites. We then calculate and visualise the location-specific model uncertainty through confidence intervals via a bootstrapping approach. In addition to providing modelling/visualisation alternatives for similar applications, this work is important for the case study site, as the Broadwater is characterised by a developed, heterogeneous catchment, within one of the fastest growing regions of Australia. Such tools, complementary to traditional monitoring programs, can yield more expansive spatial coverage of water quality variations in different areas over time without significantly increasing program costs, and provide valuable knowledge to inform catchment-based and recreational water management.

## 2. Methods

### 2.1. Study location

The Broadwater (Fig. 1) is a micro-tidal estuarine lagoon, 25 km in length on a north-south direction with depths up to approximately 8 m and several areas characterised by exposed sandy banks (Dunn et al., 2022). Catchment and river flow inputs originate from the Nerang, Coomera, Pimpama and Logan-Albert rivers, as well as from local creeks – Biggera and Loders, which can greatly influence water quality inputs. However, outside of wet weather events, tidal inputs usually exceed, in magnitude, riverine discharge volumes (Moss and Cox, 1999). Physicochemical parameters are typically affected by tidal variations for periods with little to no rainfall (Dunn et al., 2007b; Dunn et al., 2003) Nevertheless, from a water quality perspective, local rivers still play an important role as they drain numerous catchments totalling approximately 112,000 ha, which greatly vary in land use, from developing urban areas to agricultural and grazing areas, dense subtropical rainforest and industrial areas. Land use change is, at the time of writing, occurring only in the Pimpama/Stapylton region, while for the other areas in the catchment, population density has been increasing but without causing further land use changes. Regulated recycled water from four sewage treatment plants is released from diffusers during ebb tide conditions within the Gold Coast Seaway (Kaminski et al., 2018). The strategic tidally staged release is designed to maximise the hydraulic efficiency of the release system, by directing recycled water away from the Broadwater on the ebb tide, enabling assimilation into the environment within the Coral Sea with minimal impact to the Broadwater.

**Table 1**
Models details for TSS prediction. Accuracy is for calibration and, in brackets, for the validation with the LOOCV approach.

| Cluster # | Sampling sites # | Model | Accuracy |
|---|---|---|---|
| 1 | 1, 2, 3, 4, 5 | TSS = 0.0919*R1–0.0579*R2 + 6.57 | $R^2$ = 0.47 (0.42) |
| 2 | 7, 8, 9, 10, 11, 12, 13 | TSS = 0.073*B8 + 0.037*B2/B4 + 7.403*TCARI-5.403*NDWI + 3.22 | $R^2$ = 0.61 (0.38) |
| 3 | 6, 16 | TSS = 0.007528*B2 + 0.039496*B4–0.06714*B8 + 0.02636*B8/B4–1.718*TCARI-8.9588*NDWI + 11.71 | $R^2$ = 0.67 (0.22) |
| NA | 15 | TSS = 0.56*(−154*TCARI + 169*NDWI-0.04*B8/B4–2.05*B2/B4)-2.6 | $R^2$ = 0.68 (0.17) |

**Table 2**
Models details for *chl-a* prediction. Accuracy is for calibration and, in brackets, for the validation with the LOOCV approach.

| Cluster # | Sampling sites # | Model | Accuracy |
|---|---|---|---|
| 1 | 2, 5, 6, 14, 16, 17 | Chl-a = 0.0163*B4 + 0.0175*(B3/B4) + 0.528 | $R^2$ = 0.40 (0.42) |
| 2 | 1, 3, 4, 7, 8, 9, 11, 13 | Chl-a = 24.93*exp(0.0092*(NDWI-GRDI))-2.32 | $R^2$ = 0.64 (0.58) |
| NA | 12 | Chl-a = 2.89*(0.1*B8–10*R3)-7.19 | $R^2$ = 0.75 (0.22) |

The Broadwater has significant ecological, economic, and cultural importance and due to the rapid urban expansion of the region, particular attention is required to ensure the infrastructure upgrades are performed in accordance with environmental regulations. As such, the area has been the focus of a number scientific and monitoring efforts, summarised in Dunn et al. (2022), in addition to the work presented in their own paper. Water quality prediction models have also been established (e.g. Bertone et al. (2019)), to facilitate recreational waters' safety.

### 2.2. Data collection and preprocessing

To develop an empirical retrieval model, the two main sources of data needed are (1) in-situ historical water quality data, to use for model development/validation, and (2) near-synchronous satellite images (Topp et al., 2020).

For this study, free-access images were acquired by the Sentinel Multispectral Instrument (MSI) installed in the twin Sentinel-2 2A and 2B satellite platforms from the European Space Agency's (ESA) Copernicus Open Access Hub for April–October 2023 and thereafter Copernicus Data Space Ecosystem, https://dataspace.copernicus.eu/. Level 2A (processed) images were utilised as part of this study, with atmospherically corrected Surface Reflectance (SR) ortho-images with an extension of 110 × 110 $km^2$ in UTM projection WGS84 Datum. Images with cloud cover >9 % were not included in the analysis. Images were retained for analysis if the retrieval date was up to 2 days (or 3 days for the infrequent, high TSS and *chl-a* concentrations sampling days) from the in-situ sample collection date. Data from this hub (including the updated version) with the above-mentioned filtering and processing criteria were available from December 2018.We also considered an integration of relevant Landsat imagery synchronous data in the EO Browser platform from the Sentinel Hub (Sentinel_Hub, 2023); however, further retrieval was minor and limited to sampling days with negligible concentrations of TSS and *chl-a*. As such, for consistency, only Sentinel-2 products were used for this study. To convert the measurements from 16-bit integers to reflectance values between 0 and 1, the conversion equation provided by European Space Agency (2023) was applied, with quantification and offset values retrieved for each image.

In-situ water quality data used for model development, during this study, was collected through a City of Gold Coast-funded monitoring program described in Dunn et al. (2022). The locations of the sampling sites are illustrated in Fig. 1. The monitoring dataset included measurement of 14 WQPs (in particular, TSS and *chl-a*) at 18 different sampling sites in the Gold Coast Broadwater from 2016 to 2021. The sampling sites are representative of local specific features, such as rivers/creeks outflows, oceanic exchange, or foreshore developments. The collection frequency was fortnightly to monthly and as such, the overall number of WQP observations (i.e., data points) ranged from 1608 to 1795 depending on the parameter (excluding salinity, with

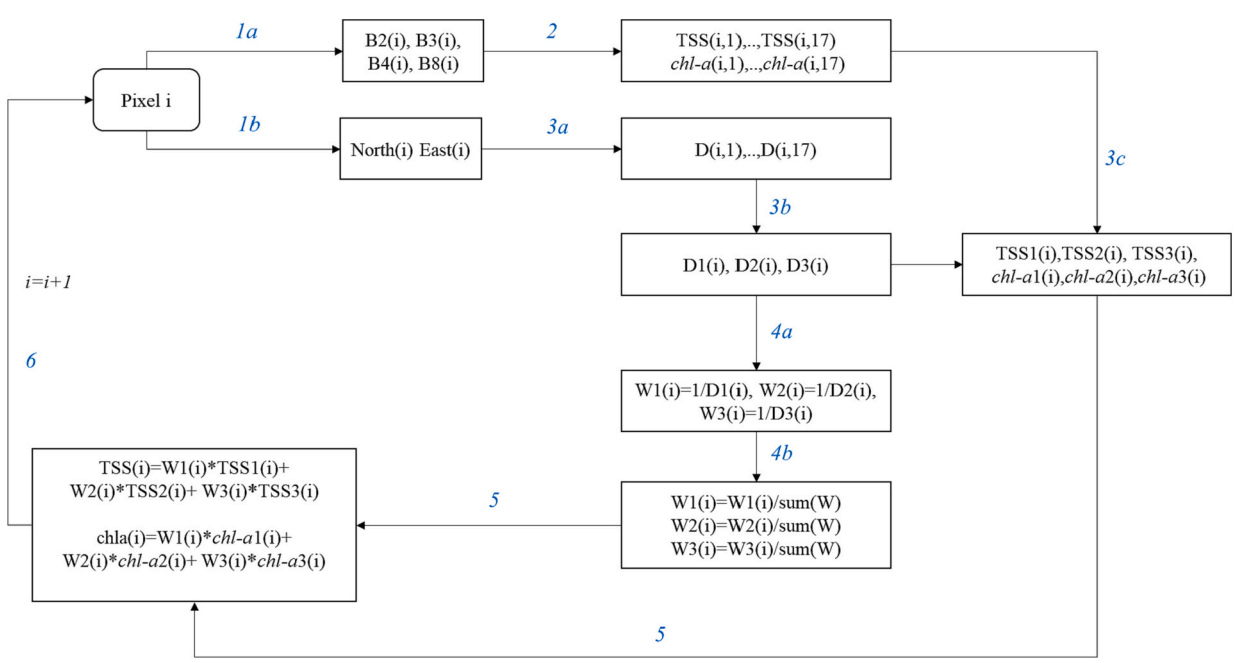


**Fig. 2.** Methodological framework of the spatially weighted average approach to pixel-specific TSS and *chl-a* prediction. In blue the process numbers as explained in the text. (For interpretation of the references to colour in this figure legend, the reader is referred to the web version of this article.)

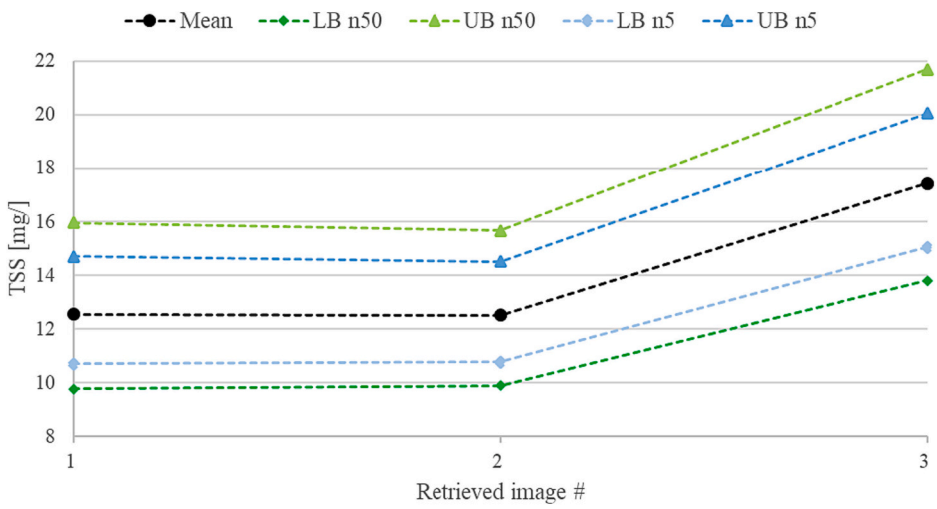


**Fig. 3.** Image-averaged TSS and 95 % confidence intervals for BI = 5 and BI = 50. LB = Lower Bound; UB = Upper Bound; n5: BI = 5; n50: BI = 50. Images dates: 1: 12/03/2019; 2: 21/01/2020; 3:15/02/2020.

1022 analyses). The total number data points for TSS and *chl-a* were 1794 and 1795, respectively (Dunn et al., 2022).

Following the data pre-processing and cleaning tasks described above for in-situ monitoring and remote sensing datasets, the number of matching data points was $n = 148$ for TSS and $n = 142$ for *chl-a* for all sites. The considerable reduction from the available in-situ dataset was due to (1) relatively low temporal frequency for both data sources, limiting the chance for same-day retrieval, (2) satellite data availability with the selected filtering/processing criteria commencing in late 2018, and (3) a number of satellite images not covering the entire Broadwater area of interest, thus missing a number of sampling sites. Such issues are not uncommon in this field (Bertone and Peters Hughes, 2023; Topp et al., 2020): the larger the existing in-situ dataset, the more likely it will be to have more synchronous readings and in turn a larger final sets of data to use for more robust model development. Given the substantially large initial dataset for this study (both in terms of time period and spatial distribution), the final number of matching data points was still deemed significant; a number of different solutions were applied, as described in the next section, to overcome remaining limitations.

### 2.3. Data analysis and model development

For the model development, a compromise between site-specificity of correlations and avoidance of model overfitting due to the small sample size (each sampling location had 6–10 matched data points only), sites clusters were developed based on similarities in their data cross-correlations and spatial proximity.

Using the Sentinel-2 data, we developed models based on both (1) reflectance values of the individual pixel matching the sampling point coordinates only, and (2) the average reflectance values for a cluster of 9 neighbouring pixels. This was because some of the sampling points are close to land; therefore, the mix of Sentinel-2 geometric accuracy and spatial resolution may lead to problems related with mixed reflectance and/or co-registration with sample points. Using a cluster of pixels approach assists removing (or correcting) land/water mixed pixels. Results show that the value of the central pixel (original one) and of the mean of the cluster do not differ by >1–2 %. This indicates that using reflectance values from only the specific pixel matching the sampling site coordinates was a reliable approach for model development within the study region.

We highlight that for this reason, and for model development purposes, we focused on the B2, B3, B4 and B8 spectral bands from Sentinel-2. While other bands (e.g. B5 to B7) may prove to be useful predictors, due to their lower spatial resolution, a more pronounced negative effect from land proximity within our study region could have occurred, since many sampling sites were located <30 m from the upper tidal limit (i.e., inter-tidal land), with some sites located at the mouth of creeks (e.g. Loders Creek, Site 17) being only approximately 20 m wide. In addition, having three additional potential predictors for an already small dataset would increase the chance of overfitting even further.

Tables 1 and 2 present the final clusters with related regression models. A combination of empirical and semi-empirical approaches was employed. We selected, as potential predictors, both the corrected reflectance values for the different relevant spectral bands (B2, B3, B4 and B8 – empirical approach), as well as combinations of them based on established ratios/indices already developed in previous well-established studies as potential indicators of TSS or *chl-a* (semi-empirical approach). Similar models for turbidity were also tested, however they yielded lower accuracy than for TSS. Variations of such existing ratios (e.g. same mathematical formulation but different spectral bands) were also tested (i.e. empirical approach). Ratios/indices retrieved from the literature include the best performing band combination used in Ouma et al. (2020) for TSS prediction from Sentinel-2, herein denoted as R1:

$$R1 = \frac{(B4 + (B8/B4))}{2} \tag{1}$$

We also included a similar format but with spectral bands B4 and B2, herein denoted as R2:

$$R2 = \frac{(B2 + (B4/B2))}{2} \tag{2}$$

Other employed indices included:

- Transformed Chl-*a* sorption in Reflectance Index (TCARI), previously proposed and used for leaf *chl-a* estimation in crops (Haboudane et al., 2002).

$$TCARI = \frac{(B4 - B8)}{(B4 + B8)} \tag{3}$$

- A similar formulation to TCARI applied to the B2 and B3 bands, herein denoted as R3.

$$R3 = \frac{B2 - B3}{B2 + B3} \tag{4}$$

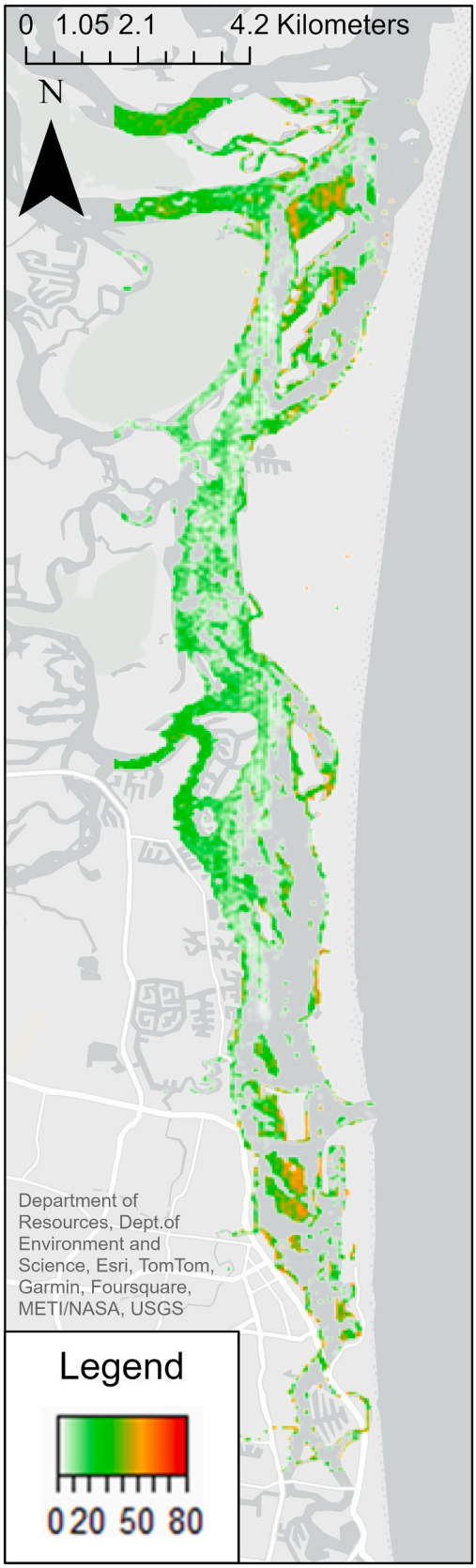


**Fig. 4.** TSS [mg/L] 97.5 % upper bound prediction difference (in percentage) among runs for BI = 50 and BI = 5 for 15/02/2020. UTM Zone 56S coordinates, WGS 84 datum (EPSG:32756) Easting and northing in metres.

- Green-Red Difference Index (GRDI), uses a slightly different version of the green-red vegetation index, and it has been used to monitor vegetation (Tucker, 1979).

$$GRDI = B3 - B4 \tag{5}$$

- Normalised Difference Water Index (NDWI), proposed to measure absorption by vegetation's liquid water (Gao, 1996) and previously used for *chl-a* prediction (Bertone and Peters Hughes, 2023).

$$NDWI = \frac{(B3 - B8)}{(B3 + B8)} \tag{6}$$

A leave-one-out cross-validation (LOOCV) approach (James et al., 2013), i.e. a particular type of cross-validation (Stone, 1978), was applied for the TSS and *chl-a* models, in order to develop the most robust model given the small datasets. LOOCV is a cross-validation technique that is specifically used to estimate how well a model will generalise to new/unseen data. Essentially similar to an "extreme" variant of a *k*-fold validation, it involves randomly splitting the dataset into training and validation sets, where each validation set contains a single data point, and the rest are used for training. This process is repeated *k* times, where $k$ = the number of data points in the dataset. The results presented in Tables 1 and 2, show that $R^2$ ranged between 0.40 and 0.75 for all models, while the value of this metric is lower for the validation test (especially for those models relying on smaller clusters). This is because the test set contains a single data point only, and hence one poor prediction might affect the overall $R^2$. The ensemble model resulting from aggregating all the models developed on the individual training set runs will presumably be more robust and yield higher accuracy over new/unseen data. Regardless, calculating the confidence intervals will help represent the uncertainty in the model's predictions.

Sites were grouped together in clusters (see Tables 1 and 2) for modelling purposes to achieve a suitable compromise between accuracy and robustness. For TSS, the first cluster contains the northernmost sites (Sites 1–5), predominantly adjacent to river entrances, which drain water from agricultural/grazing catchments. The second cluster contains sites (Sites 7–13) in the middle of the lagoon, with slightly deeper waters and different hydrodynamic/water quality influences than for the first cluster (i.e. reduced influence from river inputs). The third smaller cluster contains two river mouth sites (Sites 6 and 16) draining more urbanised catchments and in turn with potentially different features in their sediment inputs compared to the first cluster. Site 16 in particular, is receiving waters from the Nerang River, which is bounded, more upstream, by Hinze dam; this acts as a significant barrier for sediments and nutrients, thus affecting their concentrations downstream. Site 17, representing Loders Creek, could not be clustered with other sites nor could be predicted individually. Loders Creek drains a very complex, mixed-use (e.g., industrial, urban) catchment which can contribute various sources of pollutants, and in turn made a satellite-based estimation more challenging. Similarly, Site 15 could not be clustered, probably due the influence of nearby Site 17. However, an individual model of Site 15 yielded an acceptable accuracy (though lower after LOOCV validation accuracy calculation, due to the very small dataset). For *chl-a*, with the exception of Site 12, the clustering was clearer between all river entrance sites (first cluster – regardless of different land uses in the catchment) and the central estuarine lagoon sites in deeper waters less affected by river flow (second cluster). A site-specific model for Site 12 was excluded due to the poor validation accuracy (being a small dataset) and its proximity to several other monitoring sites. Instead, we applied the weighted average approach described below, similarly to any unsampled pixel. This also offered an opportunity to better validate the weighted average approach, since the three closest monitoring sites pertain to different clusters, thus leading to a unique site-specific quantification and the opportunity for validation with site-specific historical data.

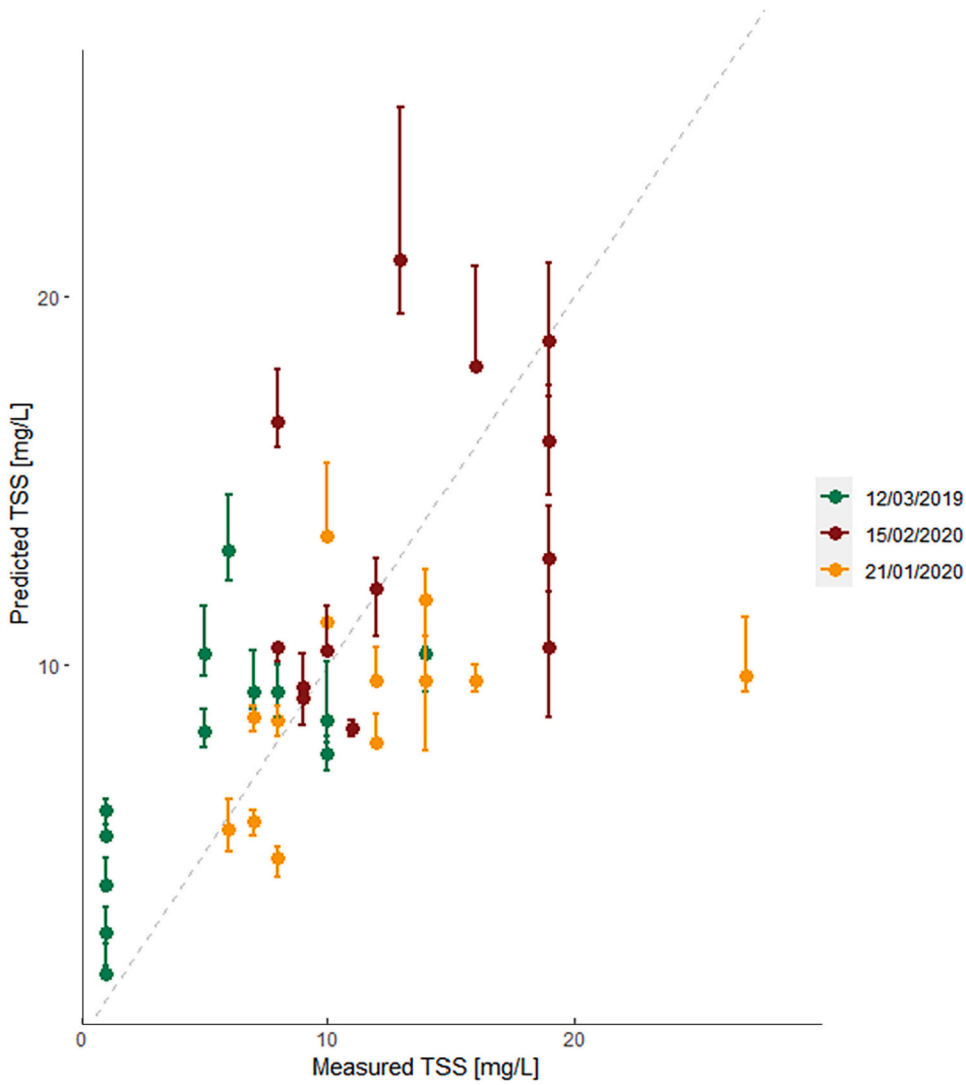


**Fig. 5.** Predicted (mean and confidence intervals from BI = 5) vs observed TSS, all sampling sites, 3 retrieval dates.

To determine the confidence intervals, a bootstrapping approach was used (Mooney et al., 1993). Bootstrapping is a statistical resampling technique used to estimate the sampling distribution of a statistic. It involves repeated sampling from observed data with replacement to create new datasets of the same size as the original dataset. This process is done many times (herein defined as bootstrapping iterations or BI) to simulate the sampling variability and generate a distribution of the statistic of interest. Bootstrapping is commonly used to calculate confidence intervals for a parameter, and this was a preferred method given the limited data (and its non-normal distribution, as clearly identifiable visually from histograms and Q-Q plots) compared to traditional confidence intervals determination methods (e.g., relying on z-values). This is important as it visually accounts for the different robustness (or lack thereof) of the site-specific models. Models built with smaller datasets would tend to have larger confidence intervals, given similar accuracy.

Finally, in order to identify which model to apply to individual pixels at unsampled locations, the proposed weighted average approach was implemented as follows and as illustrated in Fig. 2:

1. For each pixel *i*, take B2, B3, B4, and B8 processed reflectance values (1a) and extract coordinates (1b).
2. Calculate the TSS and *chl-a* predictions and confidence intervals based on reflectance values, for each sampled site based on the site/cluster-specific models.
3. Calculate the spatial distance of the pixel from each of the 17 sites (3a) and select the three closest ones (3b) – D1(*i*), D2(*i*), D3(*i*). Store the TSS and *chl-a* prediction for the three closest sites (3c) – TSS1(*i*), TSS2(*i*), TSS3(*i*) and chla1(*i*), chla2(*i*), chla3(*i*)
4. Calculate the three weights W1(*i*), W2(*i*), W3(*i*), as inversely proportional to the distance (4a) and with the sum normalised to 1 (4b).
5. Calculate the weighted average of the TSS and *chl-a* predictions at those three sites and related confidence intervals – TSS(*i*) and *chl-a* (*i*)
6. Assign that TSS and *chl-a* predicted concentrations to the pixel considered and move to the next pixel.

A series of codes were written in the R environment (Rstudio 2023.06.1 + 524), which:

1. Identify and extract B2, B3, B4, and B8 processed reflectance values, for the satellite images of interest.
2. Display both the true colour image and the individual band's reflectance values.
3. For each pixel, apply the weighted average approach described above, to generate a TSS and *chl-a* prediction and related 95 % confidence intervals based on defined BI.
4. Apply a shapefile to the predictions (calculated over the wider region captured by the satellite) for the Broadwater area to mask non-water pixels and plot the resulting image.

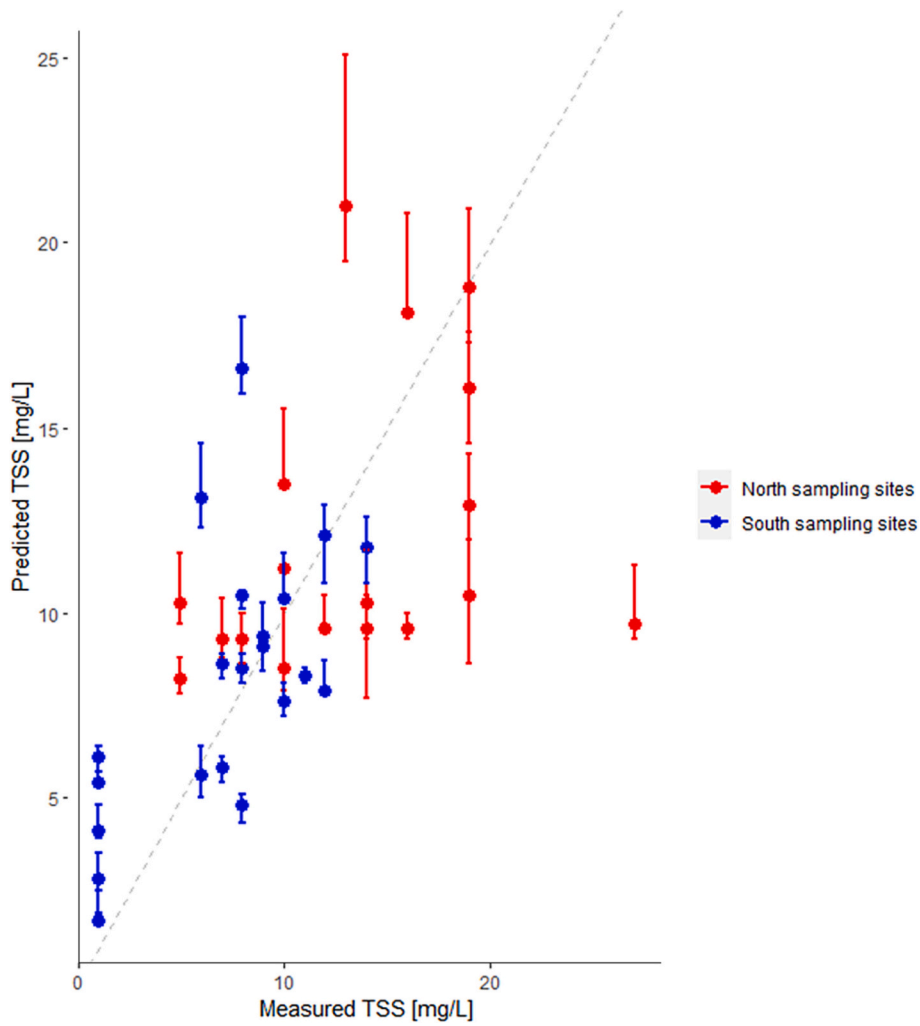


**Fig. 6.** Predicted (mean and confidence intervals from BI = 5) vs observed TSS, North/South sampling sites, 3 retrieval dates (1: 12/03/2019; 2: 21/01/2020; 3:15/02/2020) combined.

5. Extract the predicted values at the specific sampling locations.
6. Plots observations against predictions.

Due to the very high computational time required for the bootstrapping/weighted average approach, the code was run in the ARDC Nectar Research Cloud (Nectar) (https://ardc.edu.au/services/ardc-nectar-research-cloud/). The code's computational time for one individual image, which contains approximately 1.5 million pixels, increased linearly with increasing bootstrapping iterations (BI); for instance, it took ~1-day when considering BI = 5 and 10 days for BI = 50. As such, we focused our predictions on a handful (3 for TSS: 12/03/2019, 21/01/2020, 15/02/2020; 4 for *chl-a*: 12/03/2019, 21/01/2020, 15/02/2020 and 21/04/2021) of historical images. These were selected specifically as they covered both the low (12/03/2019) range as well as the high (21/01/2020, 15/02/2020, and to some extent 21/04/2021 for *chl-a*) range of observed values. We also compared the confidence intervals estimations determined with BI = 50 vs BI = 5, to understand if the discrepancy is predictable and thus allowing to run a faster code without compromising the robustness of the bootstrapping approach.

## 3. Results

Fig. 3 presents the predicted average TSS concentrations for three selected days (i.e., 1: 12/03/2019; 2: 21/01/2020; 3:15/02/2020) for the entire study region as well as the 95 % lower and upper bounds with BI = 50 and BI = 5. Fig. 3 illustrates that with increasing iterations the confidence intervals become wider. The lower bound sits, on average, 21 % below the mean for BI = 50 and 14 % for BI = 5. However, more variation (likely due to more extreme values/outliers on the upper end of concentrations) occurs for the upper bound (26 % and 16 % above the mean for, BI = 50 and BI = 5, respectively). Importantly, the differences between 5 and 50 iterations (i.e. 7 % for lower bound and 10 % for upper bound) were consistent across different images. As such, to contain the computational time, most of the subsequent analyses were run with a lower (i.e., BI = 3 or BI = 5) number of BIs and with educated assumptions/prediction of the wider confidence intervals.

While aware that this analysis was performed only on three images (out of 7 matching images) due to the extremely high computational time to run the code with BI = 50, these images included both the low and the highest range of concentrations for TSS in our dataset; the consistent output across the images provides confidence that this similar pattern would repeat itself for other retrieval dates. Fig. 4 also presents, as an example, calculation based on the 15/02/2020 satellite image (i.e., near synchronous to the sampling day with the highest TSS concentration in our dataset), specifically representing the spatially explicit differences (in percentage) between the upper bound of TSS concentration predicted with BI = 5 and BI = 50. The widespread light green colour demonstrates that the 10 %–15 % difference is consistent and uniform for most of the study area, thus indicating it is predictable. Locally higher differences were typically in proximity of land boundaries where

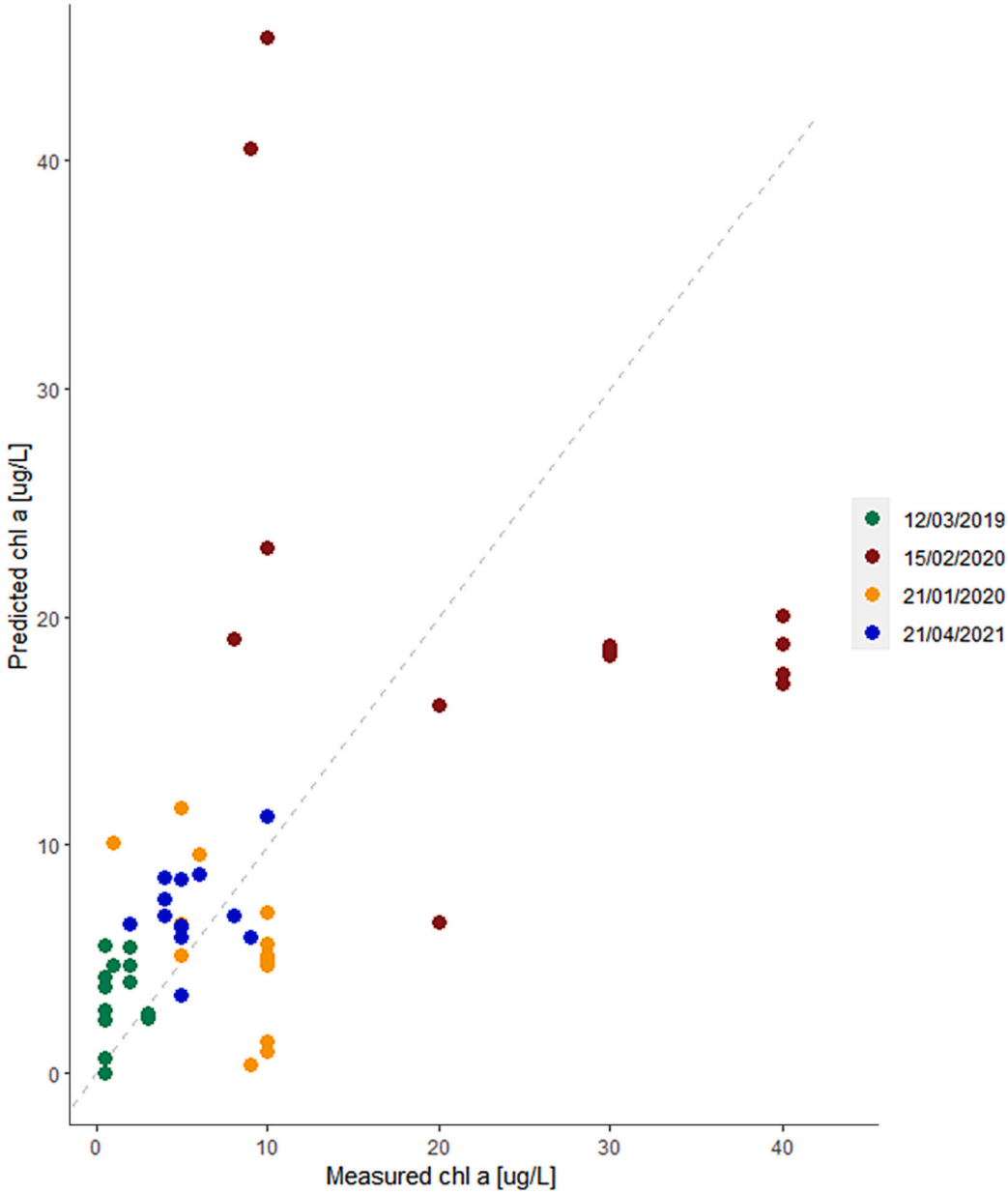


**Fig. 7.** Predicted vs observed *chl-a*, all sampling sites, 4 retrieval dates.

there is potentially higher retrieval uncertainty, and less interest for this analysis.

Figs. 5 and 6 illustrate the prediction accuracy for TSS for the three retrieval dates of interest (i.e., Images dates: 1: 12/03/2019; 2: 21/01/2020; 3:15/02/2020). Fig. 5 clusters the results based on date, while Fig. 6 presents the results based on sample location (northern vs southern region of the Broadwater). These results highlight how the February 2020 results have the highest TSS and in turn also the highest model errors. Predominantly higher concentrations were recorded at the northern sites, likely or at least partially due to being part of a model cluster with a lower calibration accuracy. While the cluster-specific accuracy was shown in Table 1, in this case it is acknowledged that overall, regardless of the cluster, the northern sites displayed the highest TSS concentrations in the dataset, which also proved more inaccurate in the predictions. While the error is most likely also due to a large discrepancy (3 days) between satellite acquisition dates and samples collection, which occurred on 18/02/2020, the confidence interval approach allows (especially when widening them according to the BI-based relationships described above) to, most times, include the true value within the 95 % confidence interval.

The authors suggest future work could focus on improving the calibration of the northern sites, through the further data collection which over time would allow a larger, synchronous, high-concentration training dataset, in turn presumably leading to more accurate predictions.

Figs. 7 and 8 present *chl-a* concentration predictions against measurements, based on retrieval date (Fig. 7) and sampling site (Fig. 8). Compared to TSS, which had a more limited number of retrieval dates with medium-high concentrations, for *chl-a* four images were considered, by adding a more recent image with mid-range concentrations. Similarly to TSS, 15/02/2020 shows a much higher variation in the predicted results compared to observations, which as mentioned before, may be due to the 3-day time lag between satellite acquisition date and sample collection. However, close scrutiny of the data reveals that most of the underpredictions are for sites where the exponential model (second cluster) was applied. This was noticed in the model development

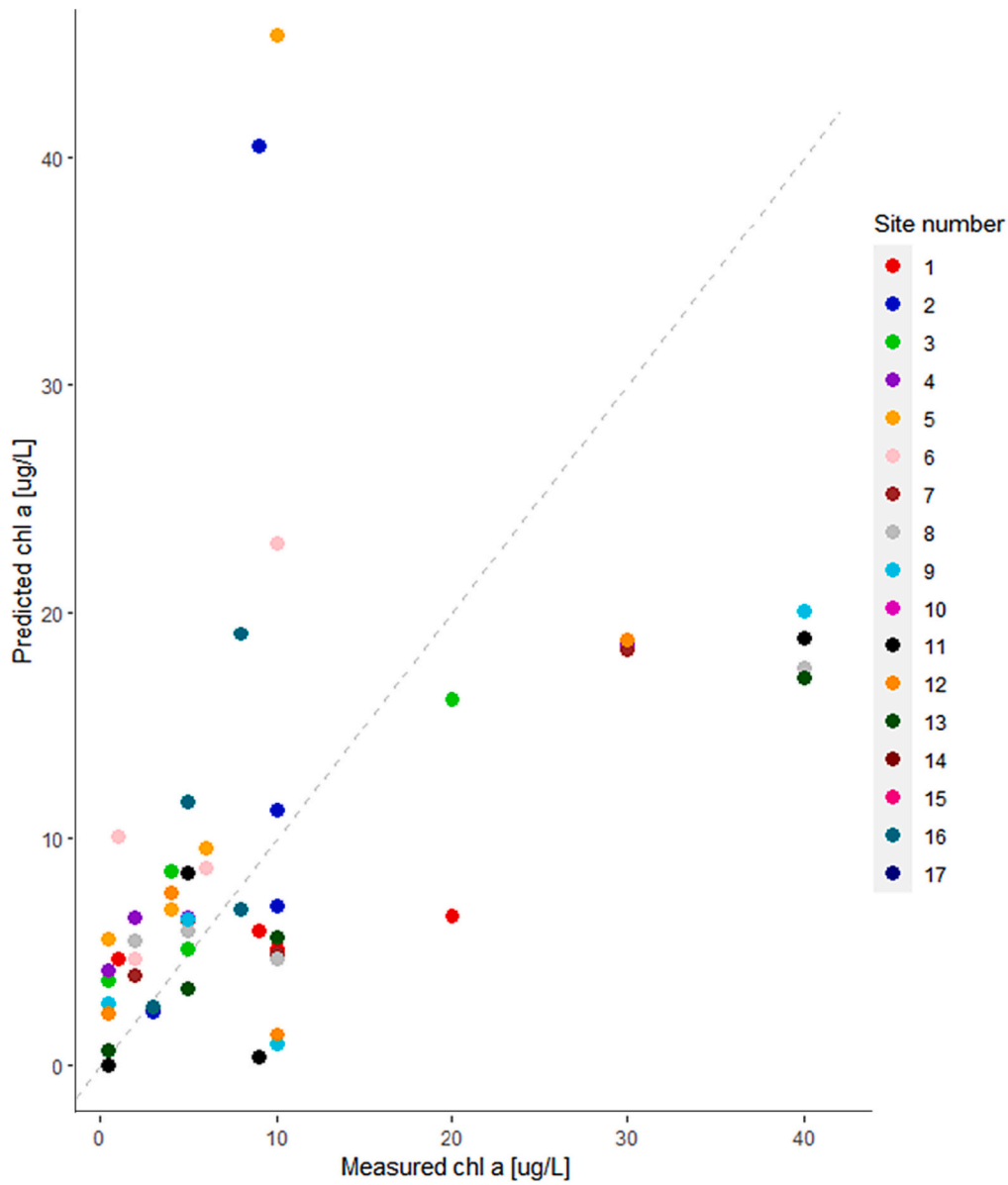


**Fig. 8.** Predicted vs observed *chl-a*, colour-coded by sampling site, 4 retrieval dates combined.

stage, with the model underpredicting within the 20–40 μg/L range. In case higher concentrations were to be recorded, the model predictions would align closer to the in-situ values.

The bootstrapping approach allowed for the inclusion of the in-situ value within the 95 % confidence intervals in most cases. For the vast majority of predictions, the in-situ value sits below the 97.5 % upper bound (Fig. 9). Hence, hypothetically, catchment managers could use the upper bound prediction to safely determine that there would be a very small (2.5 %) chance of detecting higher concentrations in the field.

To validate the accuracy/appropriateness of our weighted average approach, we compared predicted vs observed *chl-a* concentrations at Site 12 for which, as mentioned earlier, we opted to apply the weighted average approach from the three closest sites rather than an individual site-specific model. A relatively high prediction accuracy was achieved ($R^2 = 0.75$). Further work may look to focus on collecting samples from new (different) locations in the Broadwater and compare with the satellite-based estimation at the corresponding location.

Fig. 10 shows the predicted TSS concentrations for 21/01/2020 and 15/02/2020. These dates were close to the in-situ sampling days with the highest TSS readings in the historical dataset. The high concentrations were likely due to very large rainfall totals during this period, specifically: 349 mm from 12/01/2020 to 21/01/2020 and 566 mm from 4/2/2020 to 14/02/2020 recorded at the Gold Coast Seaway (BoM, 2023).

While a number of modelled results is missing from the upper section of the right panel, likely due to issues with the original satellite image, the study findings indicate the northernmost rivers were the initial (21/01/2020) and dominant contributors to TSS within the Broadwater, with elevated concentrations (i.e., >20 mg/L) occurring three weeks later in February (15/02/2020) on most the northern area of the Broadwater.

For the most critical (given the higher concentrations) February results, having the lower and upper bound estimations (Fig. 11) can assist stakeholders. For instance, the lower bound results predict that there is a 97.5 % chance that the actual TSS values are higher than those displayed in the same map. As such, in this example, a very high probability of TSS > ≈15 mg/L exist in most locations around the river entrances of the northern Broadwater. Overall, the lower and upper bounds have similar values, indicating narrow confidence intervals. This is especially valid for areas with very high (river entrances) and very low (Southern lagoon

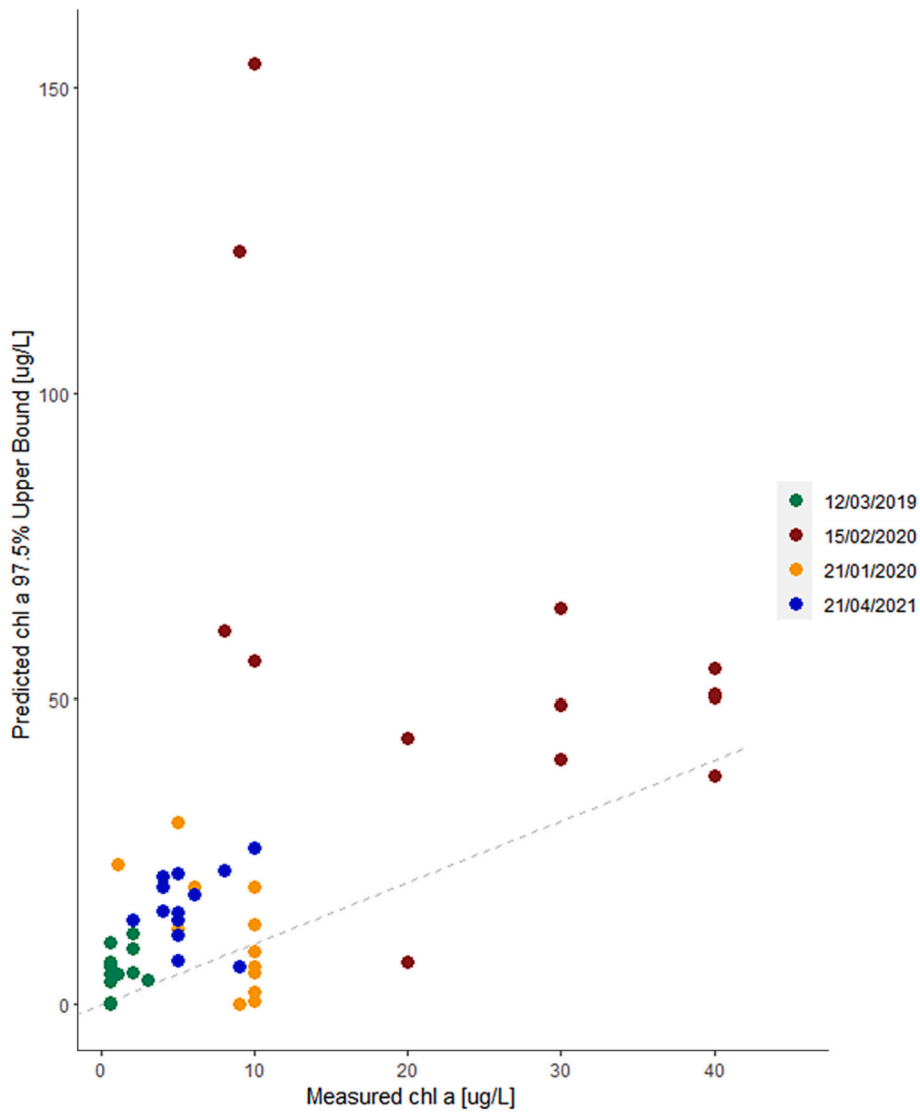


**Fig. 9.** Predicted 97.5 % upper bound (BI = 3) vs observed *chl-a*, all sampling sites, 4 retrieval dates. Slope of dashed line is 1:1.

area) TSS concentrations. Transitional regions, i.e. where the high loads coming from the rivers are diluted and mixed, show higher discrepancies, i.e. higher uncertainty in the predictions. It must be also noted that these confidence intervals were based on a code run with BI = 5. A wider (−7 %, +10 %) 95 % confidence interval would have been achieved with BI = 50.

Fig. 12 presents predicted *chl-a* concentrations during the same retrieval dates, as well as on 20/04/2021. Results associated with a high intensity rainfall recorded in early 2020 show different patterns from TSS, with early elevated *chl-a* concentrations recorded in the southern part of the Broadwater before higher concentrations were recorded in the northern region, especially within immediate receiving waters of the Coomera River. In April 2021, higher *chl-a* concentrations are present at several scattered locations, predominantly within shallow near-shore waters. Given boundary issues (e.g., mixed reflectance) were initially checked as explained (Section 2), this result may point to the presence of cyanobacteria/algae in the shallower areas of the Broadwater. While, being shallow, the readings might be partially affected by the colour and features of the sand bottom, these locations may nevertheless provide better growing conditions or may be more protected from hydrodynamic or wind-related movement, as well as receive more nutrients from the nearby rivers than other (e.g. southernmost region, receiving waters from the Nerang River) Broadwater areas. The latest, preceding significant rainfall event occurred from 4/04/2021 to 7/04/2021 (136 mm), followed by two dry weeks before the data collection date. The rainfall event may have provided nutrient inputs needed for algae to grow, in turn made possible by the subsequent relatively calm and warm conditions (water temperatures of 22–23 °C depending on the site, based on our analysis of available temperature data from the provided dataset from Dunn et al. (2022)). Further work is needed, however, to ensure the model predicts shallow areas correctly rather than misinterpreting e.g. intertidal sandbanks as regions of high concentration.

## 4. Discussion

Overall, this study contributes to the relatively limited body of work related to satellite remote sensing of estuarine lagoons, which is only a small fraction of the much larger research work completed for rivers, lakes and reservoirs (Topp et al., 2020). Regular in-situ water quality sampling and analysis within the Broadwater has, and continues to be, performed (Dunn et al., 2022). However, despite up to 18 points being recently monitored over time across the Broadwater (Dunn et al., 2022), quantification of WQP across all regions of the Broadwater remains a logistical and financial challenge. This is due to the intertidal characteristics of the water body along with the complex interactions caused by multiple inflow points and human activities (e.g. dredging and boating).

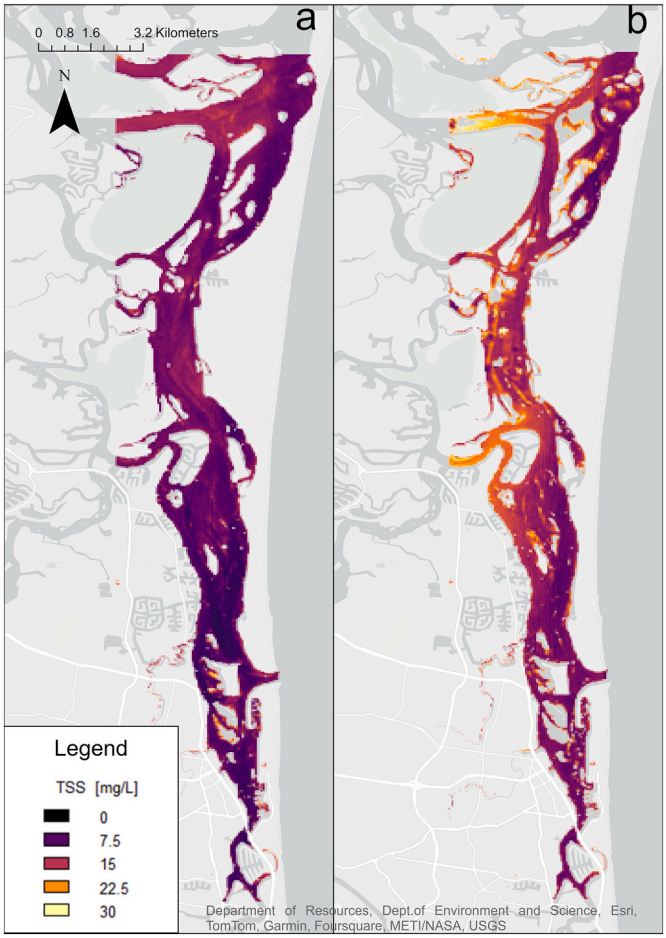


**Fig. 10.** Predicted TSS [mg/L], Broadwater, 21/01/2020 (left panel) and 15/02/2020 (right panel). UTM Zone 56S coordinates, WGS 84 datum (EPSG:32756). Easting and northing in metres.

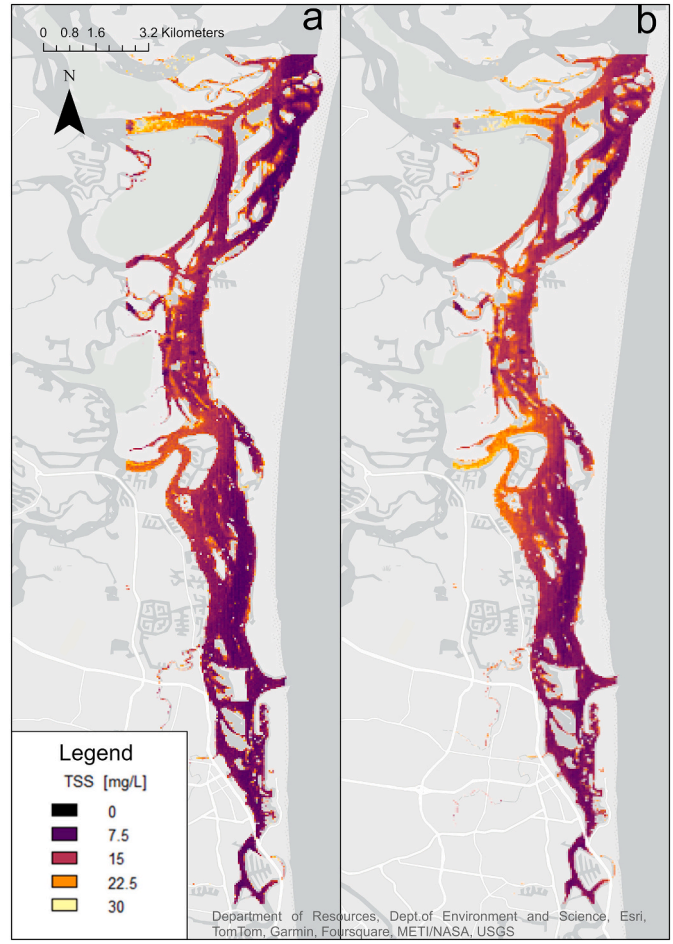


**Fig. 11.** Predicted TSS [mg/L], Broadwater, 15/02/2020; 2.5 % lower bound (BI = 5, left panel) and 97.5 % upped bound (BI = 5, right panel). UTM Zone 56S coordinates, WGS 84 datum (EPSG:32756). Easting and northing in metres.

The predicted growth in urban population and changes in land uses (especially in current agricultural areas) would likely change the spatial and temporal dynamics of sediments and associated pollutant inputs. Having a spatially explicit, and regular estimation of WQPs, such as TSS and *chl-a* concentrations, would provide new insights into TSS ad *chl-a* dynamics, as well as provide useful data for calibration or as input to existing process-based and data-driven hydrodynamic and water quality models. Such capability may also help to identify additional sites of interest to monitor using in-situ methods. At the same time, the prediction maps could be used in near-real time to issue 'trigger value' warnings if required. For instance, in recent years a potentially toxic cyanobacteria genus, called *Lyngbya maiuscula*, made its appearance in the Broadwater. High *chl-a* estimations may be due to the presence of this toxic algae and as such recreational activities might have to be restricted in such localised areas.

The proposed weighted average approach accounts for input sources having different water quality features and related optical properties. Clustering sites with similar features allows the preservation of relatively large training sets of data and, at the same time, avoiding the development of a model which is too general and does not account for the different optical properties at different locations. Despite the clusters, many datasets used for training different models were quite small; however, the application of the "leave-one-out" approach allowed for more robust models to be developed despite the data limitations; concurrently, the deployed bootstrapping approach helped to quantify confidence intervals and in turn provide, as the name implies, higher confidence with the end-user on the likely prediction range. In addition to the small dataset, other sources of errors and uncertainty include:

(1) *Uncertainty around the actual water quality values at the specific day/time of satellite retrieval.* Often, there were up to 2/3 days of gap between the in-situ sample collection and the satellite image retrieval. Using only same-day synchronous data would have limited the dataset size even further (by 87 % for same-day only, or 37 % with a 1-day allowance only). Based on expert consultation and educated assumptions, we included all those slightly asynchronous (up to 3 days) images to extend the dataset, whenever gradual TSS and *chl-a* variations could have been expected (e.g., no significant rainfall during that time gap). However, in some cases some significant variations at some sites could have occurred during that timeframe. Of particular significance in this regard is the February 2020 data, collected (18/02/2020) 3 days after the satellite retrieval (15/02/2020). This was the longest allowed time gap in our matched dataset, as it was one of the few days with high readings, and as such it was important to include it for our modelling. Results show higher errors for this particular day compared to any other analysed date. To further add uncertainty is the role of tidal variation on water quality fluctuations, which can further add discrepancy if the tide phase was different at the time of collection of the in-situ and satellite data. The use of continuous in situ water quality monitoring instruments as well as in situ radiometers would allow the creation of a much larger dataset of synchronous readings; however, the financial viability of these expensive tools might rely on multiple

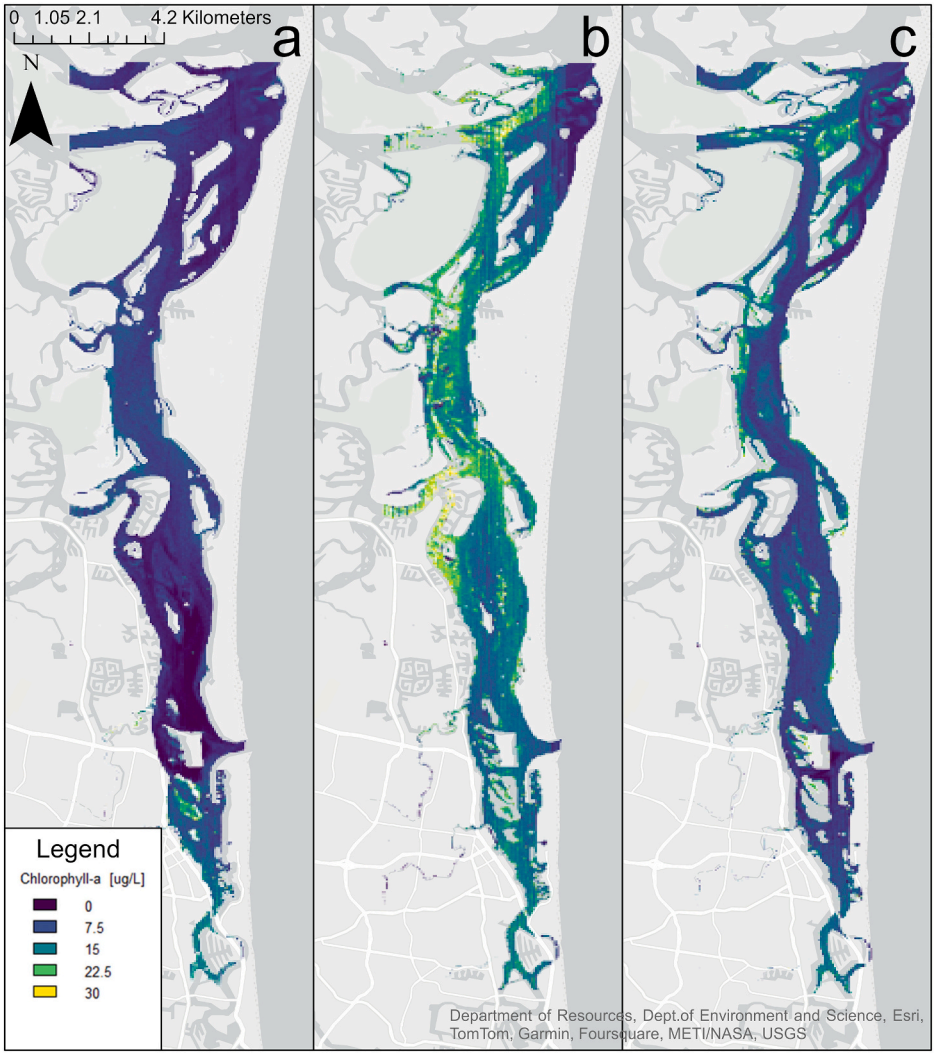


**Fig. 12.** Predicted *chl-a* [ug/L], Broadwater, 21/01/2020 (left panel) 15/02/2020 (centre panel), and 20/04/2021 (right panel). UTM Zone 56S coordinates, WGS 84 datum (EPSG:32756). Easting and northing in metres.

applications (i.e. beyond the creation of a larger dataset for this specific satellite project only).

(2) *Uncertainty around satellite data quality and quantity*. Despite applying the appropriate corrections and checking potential boundary issues, in particular for those sampling sites closer to shore, the processed reflectance values might still be not completely reliable. Alternate (current and future) available processing/correction algorithms could be investigated in future works. Also, we relied on only those relevant spectral bands having a 10 m × 10 m spatial resolution (given the proximity to land of many sampling sites). Several *chl-a* and TSS indices and algorithms rely only on combinations of these bands, namely B2, B3, B4, B8. Nevertheless, other studies have shown that other spectral bands (e.g. B5, B6, B7, with a 20 m × 20 m resolution) have potential to provide useful information for improved retrieval accuracy (Bertone and Peters Hughes, 2023; Topp et al., 2020). Future work could assess the values provided from other spectral bands, assess boundary issues such as mixed reflectance, and if results are promising, develop more accurate models, especially for certain shallow areas where the model might currently be mispredicting high *chl-a* concentrations at times. Subsequently, spatial interpolation (e.g. Bertone and Peters Hughes (2023)) approaches can be applied to still enable a 10 m × 10 m prediction resolution. For our historical dataset however, crucial limitations include the proximity of many sampling sites to land, or within relatively narrow creeks. Moving/adding sampling sites to more open water (while preserving the representativeness of the river/creek contribution), and/or the installation of in-situ sensors measuring spectral reflectance, could allow for more appropriate data collection to make use of lower resolution spectral bands.

(3) *Uncertainty around the provided lab analyses results, and in particular the precision*. Most of the high concentration results for e.g. *chl-a* were all either exactly 30 μg/L or 40 μg/L. While the original collected data might have had a higher level of precision, the lack of it in the provided data is herein acknowledged, though playing a more minor role compared to the other mentioned points.

(4) *Limited dataset at high concentrations*. It is well known that satellite retrieval of water constituents is more difficult when their concentrations are low, due to lower signal to noise ratio. At the same time, most of the poor water quality events occur in summer, due to higher water temperatures and wet weather events. Unfortunately, these periods often coincide with rainy/overcast weather. The high cloud cover does not allow for accurate correction/processing of reflectance values and as such the amount of synchronous data for such high-concentration events grows much more slowly than for the low concentrations (i.e., dry weather) data.

Despite the limitations, this research work has introduced a number of methodological concepts which, when combined within the overall methodological framework of Fig. 2 and Section 2.3 with their specific objectives, provides elements of novelty in this field. To summarise, this includes (1) avoiding the issue of limited data with sampling site specific predictions, as well as the issue of non-generalisability and thus poor accuracy of a whole-lagoon model, by instead forming a handful of site clusters based on similar optical properties; (2) generating confidence intervals maps with a bootstrapping approach given the features of the historical data; (3) ensuring model accuracy and robustness in spite of limited data, with a leave one out cross validation approach; and (4) estimation of TSS and *chl-a* at any unsampled site based on a weighted average approach, averaging the modelling predictions for the three closest sampling sites. All these elements combined, provided an effective, novel and robust method to predict water quality for the Broadwater, based on local features and data availability.

Overall, given the empirical (i.e., data-driven) modelling approach deployed, further in-situ data collection, potentially also at different sites and with newer technologies, would address most of the aforementioned issues and gradually improve accuracy over time. A larger dataset might also enable other means of calculating the confidence intervals, as the bootstrapping approach (with large BI) proved to be very computationally intensive.

## 5. Conclusions

The Broadwater is an estuarine lagoon draining a complex mixed-use and rapidly changing catchment. Satellite retrieval of important water quality constituents such as TSS and *chl-a* provides an inexpensive and time-effective means to complement in-situ water quality monitoring efforts and better understand their spatial variability. In this work, we combined empirical/semi-empirical retrieval approaches for this goal. Sampling sites were grouped in clusters based on similarities, and for each cluster a retrieval model was developed.

A weighted-average approach based on closest sampling sites was used to estimate TSS and *chl-a* concentrations at unsampled locations. A leave-one-out approach was used to ensure model robustness, despite the limited dataset, and a bootstrapping approach was deployed to estimate confidence intervals in light of the non-normal distribution of the historical data. Overall, WQP concentration estimation accuracy was acceptable and varied according to the model/cluster. Furthermore, confidence interval maps can aid ends users to understand uncertainty behind the estimation and take decisions accordingly (e.g., limit recreational water use; conduct ad-hoc intensive sampling, etc).

This study offers insights on the dynamic shifts in water quality across the Broadwater, particularly in response to wet weather events. During the primary event scrutinised, the TSS concentrations observed were more elevated in the river entrances situated in the northernmost regions. In contrast, *chl-a* concentrations exhibited an initial increase in the southernmost areas, highlighting a distinct spatial and temporal pattern in the impact of environmental factors on water quality dynamics.

Future research could take advantage of further years of data collection to refine the models and potentially include other spectral bands as well as data from other satellite missions. The retrieved water quality maps could also be used to calibrate/validate process-based models, which could then be deployed to inform stakeholders of potential water quality changes following certain land use changes, new developments, or more extreme weather events.

## CRediT authorship contribution statement

**Edoardo Bertone:** Writing – original draft, Visualization, Validation, Software, Project administration, Methodology, Investigation, Formal analysis, Data curation, Conceptualization. **Andrea Ajmar:** Writing – review & editing, Validation, Supervision, Methodology. **Fabio Giulio Tonolo:** Writing – review & editing, Methodology(remote sensing dataset). **Ryan J.K. Dunn:** Writing – review & editing, Resources. **Nicholas J.C. Doriean:** Writing – review & editing, Visualization, Validation, Resources. **William W. Bennett:** Writing – review & editing, Resources. **Jemma Purandare:** Writing – review & editing, Resources.

## Declaration of competing interest

The authors declare that they have no known competing financial interests or personal relationships that could have appeared to influence the work reported in this paper.

## Data availability

Some of the historical water quality data was collected by City of Gold Coast and would require permission from them to be shared. Model code and results can be made available on request

## Acknowledgments

The first author is grateful to Isaac Jennings from Griffith University, for facilitating access and setup of the ARDC Nectar Research Cloud to remotely run the developed R codes. Additionally, the measured in situ WQP data utilised during this study was acquired during works undertaken by the Coastal and Marine Research Centre (CMRC) Griffith University under the 'Baseline Water Quality Monitoring Program' project funded by the City of Gold Coast (LG314/621/20/158), initiated by Anna Hollingsworth, and managed by Jemma Purandare, and Kathy Baker of the City of Gold Coast Environment, Heritage, and Resilience Department.

## References

Bertone, E., Peters Hughes, S., 2023. Probabilistic prediction of satellite-derived water quality for a drinking water reservoir. Sustainability 15 (14), 11302.

Bertone, E., Purandare, J., Durand, B., 2019. Spatiotemporal prediction of Escherichia coli and enterococci for the commonwealth games triathlon event using Bayesian networks. Mar. Pollut. Bull. 146, 11–21.

Bohn, V.Y., Carmona, F., Rivas, R., Lagomarsino, L., Diovisalvi, N., Zagarese, H.E., 2018. Development of an empirical model for chlorophyll-a and Secchi Disk Depth estimation for a Pampean shallow lake (Argentina). Egypt. J. Remote Sens. Space Sci. 21 (2), 183–191.

BoM 2023 Climate Data Online. Bureau of Meteorology, A.G. (ed).

Cherukuru, N., Martin, P., Sanwlani, N., Mujahid, A., Müller, M., 2020. A semi-analytical optical remote sensing model to estimate suspended sediment and dissolved organic carbon in tropical coastal waters influenced by peatland-draining river discharges off Sarawak, Borneo. Remote Sens. 13 (1), 99.

Dall'Olmo, G., Gitelson, A.A., Rundquist, D.C., Leavitt, B., Barrow, T., Holz, J.C., 2005. Assessing the potential of SeaWiFS and MODIS for estimating chlorophyll concentration in turbid productive waters using red and near-infrared bands. Remote Sens. Environ. 96 (2), 176–187.

Duan, H., Ma, R., Xu, J., Zhang, Y., Zhang, B., 2010. Comparison of different semi-empirical algorithms to estimate chlorophyll-a concentration in inland lake water. Environ. Monit. Assess. 170 (1), 231–244.

Dunn, R.J., Teasdale, P.R., Warnken, J., Schleich, R.R., 2003. Evaluation of the diffusive gradient in a thin film technique for monitoring trace metal concentrations in estuarine waters. Environ. Sci. Technol. 37 (12), 2794–2800.

Dunn, R., Ali, A., Lemckert, C., Teasdale, P., Welsh, D., 2007a. Short-term variability of physico-chemical parameters and the estimated transport of filterable nutrients and chlorophyll-a in the urbanised Coombabah Lake and Coombabah Creek system, southern Moreton Bay, Australia. J. Coast. Res. 1062–1068.

Dunn, R., Teasdale, P., Warnken, J., Jordan, M., Arthur, J., 2007b. Evaluation of the in situ, time-integrated DGT technique by monitoring changes in heavy metal concentrations in estuarine waters. Environ. Pollut. 148 (1), 213–220.

Dunn, R., Catterall, K., Hollingsworth, A., Kirkpatrick, S., Capati, G., Hudson, S., Khan, S., Panther, J., Stuart, G., Szylkarski, S., 2012. Short-term variability of nutrients and fecal indicator bacteria within the Gold Coast seaway, southern Moreton Bay (Australia). J. Coast. Res. 28 (1A), 80–88.

Dunn, R.J.K., Doriean, N.J.C., Bennett, W.W., Welsh, D.T., Purandare, J., Tomlinson, R. B., 2022. Baseline water quality of the Gold Coast Broadwater, southern Moreton Bay (Australia). Mar. Pollut. Bull. 185, 114234.

European Space Agency, 2023. Level-2A Product Formatting. https://sentinels.copernicus.eu/web/sentinel/technical-guides/sentinel-2-msi/level-2a/product-formatting. (Accessed 31 May 2023).

Gao, B.-c., 1996. NDWI—a normalized difference water index for remote sensing of vegetation liquid water from space. Remote Sens. Environ. 58 (3), 257–266.
Haboudane, D., Miller, J.R., Tremblay, N., Zarco-Tejada, P.J., Dextraze, L., 2002. Integrated narrow-band vegetation indices for prediction of crop chlorophyll content for application to precision agriculture. Remote Sens. Environ. 81 (2), 416–426.
Hansen, C.H., Williams, G.P., 2018. Evaluating remote sensing model specification methods for estimating water quality in optically diverse lakes throughout the growing season. Hydrology 5 (4), 62.
James, G., Witten, D., Hastie, T., Tibshirani, R., 2013. An Introduction to Statistical Learning. Springer.
Kaminski, H.L., Fry, B., Warnken, J., Pitt, K.A., 2018. Stable isotopes demonstrate the effectiveness of a tidally-staged sewage release system. Mar. Pollut. Bull. 133, 233–239.
Kutser, T., Pierson, D.C., Kallio, K.Y., Reinart, A., Sobek, S., 2005. Mapping lake CDOM by satellite remote sensing. Remote Sens. Environ. 94 (4), 535–540.
Li, S., Song, K., Wang, S., Liu, G., Wen, Z., Shang, Y., Lyu, L., Chen, F., Xu, S., Tao, H., Du, Y., Fang, C., Mu, G., 2021. Quantification of chlorophyll-a in typical lakes across China using Sentinel-2 MSI imagery with machine learning algorithm. Sci. Total Environ. 778, 146271.
Markogianni, V., Kalivas, D., Petropoulos, G.P., Dimitriou, E., 2018. An appraisal of the potential of Landsat 8 in estimating chlorophyll-a, ammonium concentrations and other water quality indicators. Remote Sens. 10 (7), 1018.
Mooney, C.Z., Duval, R.D., Duvall, R., 1993. Bootstrapping: A Nonparametric Approach to Statistical Inference. Sage.
Moss, A., Cox, M., 1999. Southport Broadwater and Adjacent Pacific Ocean: Water Quality Study 1979–1998. Queensland Department of Environment.
Ouma, Y.O., Noor, K., Herbert, K., 2020. Modelling reservoir chlorophyll-a, TSS, and turbidity using sentinel-2A MSI and Landsat-8 OLI satellite sensors with empirical multivariate regression. J Sens 2020, 8858408.
Roncoroni, M., Mancini, D., Kohler, T.J., Miesen, F., Gianini, M., Battin, T.J., N Lane, S., 2022. Centimeter-scale mapping of phototrophic biofilms in glacial forefields using visible band ratios and UAV imagery. Int. J. Remote Sens. 43 (13), 4723–4757.
Sagan, V., Peterson, K.T., Maimaitijiang, M., Sidike, P., Sloan, J., Greeling, B.A., Maalouf, S., Adams, C., 2020. Monitoring inland water quality using remote sensing: potential and limitations of spectral indices, bio-optical simulations, machine learning, and cloud computing. Earth Sci. Rev. 205, 103187.
Seegers, B.N., Werdell, P.J., Vandermeulen, R.A., Salls, W., Stumpf, R.P., Schaeffer, B.A., Owens, T.J., Bailey, S.W., Scott, J.P., Loftin, K.A., 2021. Satellites for long-term monitoring of inland U.S. lakes: the MERIS time series and application for chlorophyll-a. Remote Sens. Environ. 266, 112685.
Sentinel_Hub, 2023. EO Browser.
Stone, M., 1978. Cross-validation: a review. Statistics: J. Theor. Appl. Stat. 9 (1), 127–139.
Topp, S.N., Pavelsky, T.M., Jensen, D., Simard, M., Ross, M.R., 2020. Research trends in the use of remote sensing for inland water quality science: moving towards multidisciplinary applications. Water 12 (1), 169.
Tucker, C.J., 1979. Red and photographic infrared linear combinations for monitoring vegetation. Remote Sens. Environ. 8 (2), 127–150.
Werther, M., Odermatt, D., Simis, S.G.H., Gurlin, D., Lehmann, M.K., Kutser, T., Gupana, R., Varley, A., Hunter, P.D., Tyler, A.N., Spyrakos, E., 2022. A Bayesian approach for remote sensing of chlorophyll-a and associated retrieval uncertainty in oligotrophic and mesotrophic lakes. Remote Sens. Environ. 283, 113295.